AIAA JOURNAL
Vol. 39, No. 1, January 2001

Drag Reduction of Afterbodies by Controlled Separated Flows

P. R. Viswanath*
National Aerospace Laboratories, Bangalore 560 017, India

The zero-lift drag characteristics of a class of multistep afterbodies that utilize the concept of controlled separated flows are documented at transonic and supersonic speeds. The important geometrical and flow parameters affecting the drag of such afterbodies are identified, and their effects are examined through a parametric study. The results show that multistep afterbodies can be designed that provide significant total drag reduction (as high as 50%) compared to (unmodified) blunt bases; however, compared to axisymmetric boattailed afterbodies of a given base area, the multistep afterbodies have relatively higher drag. Finally, the certain flow features involving separation and reattachment on multistep afterbodies are discussed based on flow visualization studies.

Nomenclature

A_b	=	base area
A_f	=	forebody area
C_{DA}	=	afterbody total drag coefficient, drag force/$(q_\infty * A_f)$
C_{DB}	=	base drag coefficient, base drag/$(q_\infty * A_f)$
C_{DP}	=	afterbody profile drag coefficient, $C_{DA} - C_{DB}$
C_{pb}	=	base pressure coefficient, $(p_b - p_\infty)/q_\infty$
D	=	base diameter, 16 mm
D_f	=	forebody diameter, 25 mm
h	=	step height
L	=	total length of body, 305 mm
L_a	=	length of afterbody (Fig. 2)
l	=	step length
M_∞	=	freestream Mach number
N	=	number of steps
p_b	=	base pressure
p_∞	=	freestream static pressure
q_∞	=	freestream dynamic pressure
Re_L	=	freestream Reynolds number based on L
x_R	=	average distance to reattachment from step face
β	=	boattail angle
δ_0^*	=	displacement thickness ahead of step
θ_0	=	momentum thickness ahead of step

I. Introduction

THE problem of turbulent base flows and the drag associated with them has been of considerable interest in projectile, missile, and combat aircraft design. Numerous studies in the literature have been devoted to reducing base drag in both two-dimensional and axisymmetric cases.[1,2] Methods that have been found effective on axisymmetric bodies include boattailing,[3] base bleed,[4] base combustion,[5] locked vortex afterbodies,[6] and ventilated cavites.[7] On axisymmetric bases, because the vortex shedding phenomenon is relatively weak (unlike on two-dimensional bases), it has been argued[2] that base drag reduction results primarily from the alteration of the mean flow caused by the device.

It was shown by Kentfield[8] that a multistep afterbody (Fig. 1) that utilizes the concept of controlled separated flows can offer significant drag reduction; he found 60% base drag reduction compared to an (unmodified) blunt base using a three-step model at low speeds. Stepped afterbodies result in a number of toroidal vortices, and in a broad sense, they may be identified with "separation control by trapped vortices" discussed by Ringleb,[9] with one major difference. For achieving drag reduction, the vortices generated at the annular steps have to be weak in contrast with a strong vortex, which is a major feature of separation control using a standing or a trapped vortex; locked afterbodies,[6] which involve a stable vortex between the base and a circular disk mounted downstream, utilize this concept.

Encouraged by the results of Kentfield,[8] Wikoff et al.[10] examined the effectiveness of the stepped afterbody concept on a spin stabilized 20-mm-diam projectile in a ballistic range. Three configurations, namely, a flat base, a stepped afterbody, and a truncated boattail ($\beta = 7.3$ deg), were tested in the Mach number range of 0.52–3.14. The results for zero-lift drag demonstrated that, whereas the stepped afterbody offered lower drag compared to the flat base, the boattailed base was more effective in reducing the drag further by approximately 20%. The performance of the stepped afterbody concept was further examined by Kidd[11] on a fin-stabilized missile model (which is a clean configuration unlike the projectile geometry with rotating bands used by Wikoff et al.[10]) in a free-flight aeroballistic range in the Mach number range 0.6–1.16. Nine different stepped afterbodies (see Ref. 11 for further details), in addition to a flat base, were tested. The stepped afterbody (configuration E), which gave the highest drag reduction (approximately 14%) compared to the flat base, was found to be less effective compared to a truncated boattail base having the same convergence angle and afterbody length as configuration E. The results of Wikoff et al.[10] and Kidd[11] broadly suggest that stepped afterbodies may not be as effective as boattailed afterbodies in reducing the base drag; however, in their work, the boattailed and multistep afterbodies had different base areas and, therefore, drag comparisons can be only be viewed as approximate.

The earlier studies[10,11] appear to have been motivated by design applications, and little information exists on the parameters that may influence the drag of such stepped afterbodies. As a result, the benefits that are realizable from multistep afterbodies have not emerged from earlier work.

In this paper, an attempt has been made to the study the zero-lift drag characteristics of a class of multistep afterbodies at transonic and supersonic Mach numbers. The stepped afterbodies have been chosen to have a common step height and uniform spacing. The important geometrical and flow parameters relevant to the design of such afterbodies have been identified, and a parametric study has been conducted assessing the different effects. The drag characteristics of multistep afterbodies have been compared with the drag of axisymmetric afterbodies[12] with circular arc and conical boattails for the same base area. The results show that multistep afterbodies do offer significant total drag reduction compared to an (unmodified) blunt base; however, compared to axisymmetric boattails of a given base area, the multistep afterbodies are less effective in providing drag reduction. Certain flow features involving separation and reattachment on stepped afterbodies are discussed based on flow visualization studies.

II. Design of Multistep Afterbodies

A multistep axisymmetric afterbody (Fig. 1) consists essentially of a number of annular backward facing steps ahead of the base. A toroidal vortex results from the separation and reattachment at each step. For achieving drag reduction, the vortex generated at each step

Presented as Paper 99-0274 at the 37th Aerospace Sciences Meeting, Reno, NV, 11–14 January 1999; received 1 October 1999; revision received 22 May 2000; accepted for publication 22 May 2000.

*Head, Experimental Aerodynamics Division. Associate Fellow AIAA.

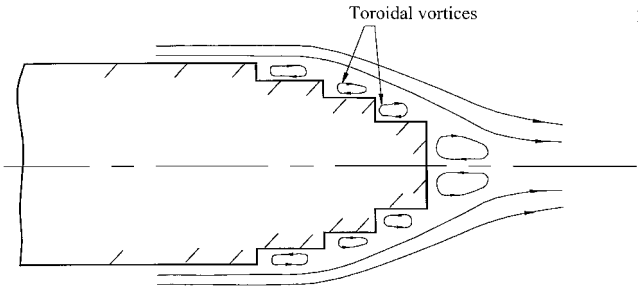

Fig. 1 Flow past a multistep afterbody.

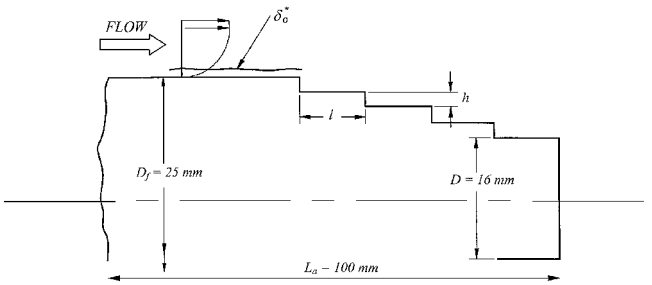

No. steps	h mm	l mm				L_a mm
8	0.560	2.5	5.0	10.0		100
4	1.125	2.5	5.0	10.0	20.0	100
2	2.250		5.0	10.0	20.0	100

Fig. 2 Geometric details of multistep afterbodies.

has to be necessarily weak so that the base drag penalty at each step can be minimized. Design of multistep afterbodies (MSA), therefore, involves selection of the right combination of step numbers and step geometry (height and spacing) for a given application.

For simplicity, we consider an idealized stepped afterbody (Fig. 2) with a common step height h and separated by a uniform distance l. As we shall see, the ratio of step length to height l/h is an important parameter in the problem because it governs shear layer reattachment. It is known that the base drag at a single back step geometry can be minimized if the step height h is chosen comparable to the boundary-layer displacement δ_0^* or momentum thickness θ_0 ahead of the step.[13,14] In the context of a multistep configuration, however, the flow is more complex, involving separation and reattachment at every step, and a relevant viscous length scale that can be used to guide the selection of step height is not known a priori. As an initial guess, we have chosen δ_0^* (or θ_0) in our analysis. With a turbulent boundary layer approaching the afterbody, the base pressure and total afterbody drag may be considered to depend on 1) flow parameters M_∞ and Re_L, 2) afterbody parameters D_f, D, h, and l, and 3) number of steps N.

With a turbulent boundary layer ahead of the base, it is appropriate to choose δ_0^* or θ_0 (just ahead of the first step) representing the Reynolds number effects. Dimensional analysis suggests

$$C_{pb} = f_1\left(M_\infty, \frac{\delta_0^*}{D_f}, \frac{D}{D_f}, \frac{l}{h}, \frac{h}{\delta_0^*}, N\right)$$

$$C_{DA} = f_2\left(M_\infty, \frac{\delta_0^*}{D_f}, \frac{D}{D_f}, \frac{l}{h}, \frac{h}{\delta_0^*}, N\right)$$

where C_{pb} and C_{DA} are normalized by forebody cross-sectional area. This provides a framework for analyzing the base and total drag characteristics of MSA.

III. Experiments

A. Test Facility

Experiments have been performed in a 30 × 38 cm trisonic wind tunnel in the Mach number M_∞ range 0.7–1.0. The transonic test section was slotted with 8% open area ratio on the top and bottom walls. The freestream Reynolds number [based on model length of 30.5 cm (Fig. 3)] varied between 8×10^6 and 9.5×10^6 in the given Mach number range. To assess the typical performance of MSA in supersonic flow, experiments were conducted at a Mach number of 2.0, and the corresponding Reynolds number Re_L was 10×10^6. The supersonic test section had dimensions of 30 × 30 cm and utilized fixed-block nozzle liners.

B. Model Support System and Balance

The model support system, along with the afterbody and drag balance, is shown in Fig. 3. The model was supported using a thin wing section between two forks of rectangular cross section, similar to that employed in many earlier investigations involving afterbody studies.[15,16] The metric part of the model (Fig. 3) consisted of a fixed cylindrical section 30 mm long and removable afterbody 100 mm long. Different afterbody models, either multistep or conventional boattails, with a length L_a of 100 mm can be fixed to the balance. The balance (designed for an axial force of 2.25 kg) measured the total drag force experienced by the metric part of the model. The model boundary layer was tripped in the nose region (using size 40 caborundum particles over a width of 3 mm) at a distance of 25 mm from the apex. Base pressure was measured on the model centerline at the last step face, using a static pressure port flush with the surface (Fig. 3).

A discussion of likely interference effects due to the model support system is appropriate. Although total elimination of model support system interference effects in the experimental study of afterbody flows in conventional wind tunnels is almost an impossible task, tremendous care was exercised in the design of the model support system, keeping in view possible transonic and supersonic interference effects. The support system was designed primarily to withstand the aerodynamic starting loads at Mach 2.0. As a result, the (maximum) solid blockage of the model including the support system at section AA (Fig. 3) was about 1.5% (about 0.5–1% is desirable). From an examination of the wave system from the body nose, fork tip, and wing leading edge and of their (corresponding) reflections from the (solid) tunnel wall, it was confirmed that the base or near-wake flow was free from wave interference at Mach 2.0 (Ref. 12). The wing–body junction is another source that can cause some degree of asymmetry of the flow over the axisymmetric body. Although this effect cannot be eliminated, due attention was given while designing the model support system (Fig. 3). Relatively thin wings, which would just meet the strength and rigidity requirements, were used to support the model. No direct check on flow axisymmetry could be made due to the relatively small thickness of the boundary layers (about 4 mm) on the body. The surface flow visualization photographs (to be discussed in Sec. IV.C), which were taken normal to the plane of the wing support, do provide some evidence that asymmetric flow features on the steps were small.

The flow inclination in the tunnel is less than 0.1 deg, and all of the measurements were made with the axisymmetric model at zero incidence. Although the support system design was such that the model would become located nominally at zero incidence, care was taken to install the model at zero incidence using an accurate inclinometer. In view of the different measures taken (discussed earlier), support interference effects are expected to be small. Furthermore, a major interest in the study is to evaluate the relative merits of MSA with axisymmetric boattails, and minor interference effects should not significantly affect the conclusions drawn.

C. Afterbody Models

The MSA investigated included a family of models with two, four, and eight steps, as shown in Fig. 2. All of the models had a length of 100 mm and base to forebody cross-sectional area of 0.41. As discussed in Sec. II, the step height has been chosen based on boundary-layer displacement thickness δ_0^* ahead of the first step. Because the boundary layer growing on the axisymmetric model is relatively thin (estimated to be about 4 mm ahead of the base), velocity profile measurements could not be made on the model. Instead, turbulent boundary-layer calculations using the lag-entrainment method of Green[17] were made, corresponding to tunnel test conditions (assuming zero pressure gradient on the body). Based on these calculations,

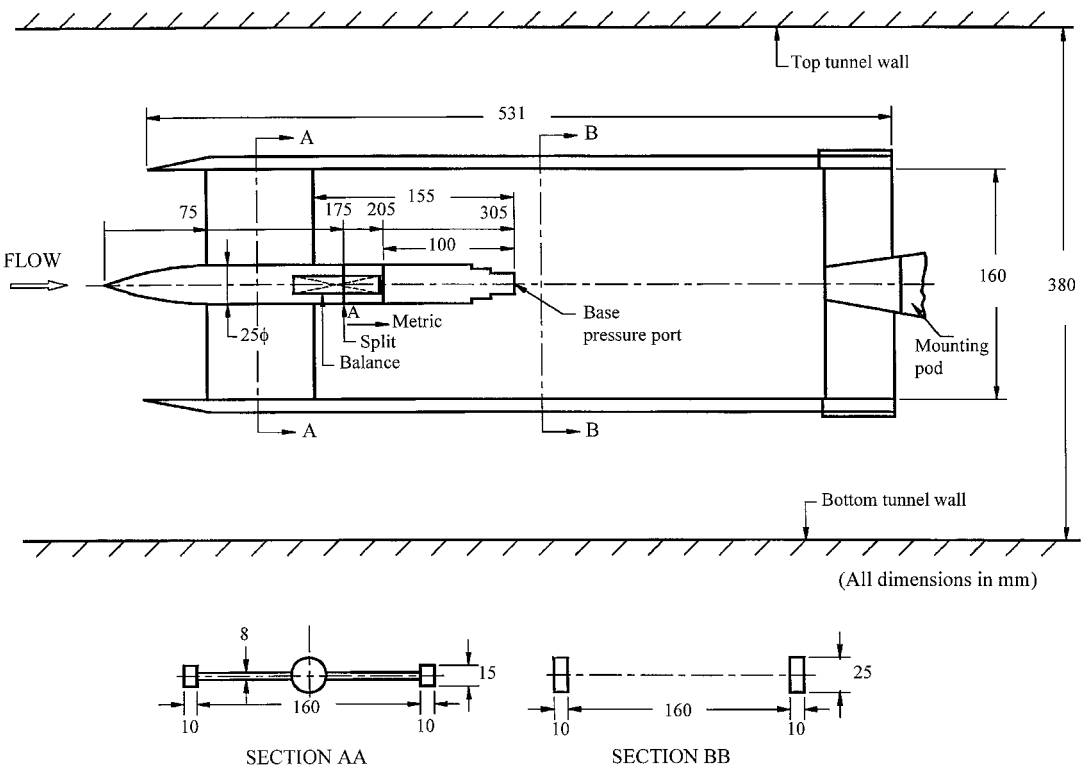

Fig. 3 Model support system, afterbody and balance.

an average value of δ_0^* of 0.55 mm at location A (Fig. 3) was chosen in the M_∞ range of 0.70–0.95; similarly, δ_0^* value of 0.80 mm was chosen at $M_\infty = 2.0$.

To provide a critical assessment of the drag reduction performance of these MSA, we have compared with the drag results obtained on axisymmetric boattails from an earlier study[12] using the same wind tunnel, model support system, and balance as shown in Fig. 3. These axisymmetric afterbodies involved both conical and circular arc profiles with different boattail angles and had the same base-to-forebody area ratio of 0.41. More details are available in Ref. 12.

D. Measurements

The measurements for each blowdown consisted primarily of outputs from the drag balance and different pressure transducers, which were acquired and processed on a personal computer 486 system. The tunnel stagnation pressure was measured with a 1035-kPa transducer. Two 17-kPa transducers were employed to measure the differences between the freestream static and the base pressure and between the freestream static and the split pressure. The split pressure was measured in the narrow gap between the metric and nonmetric portions of the model (Fig. 3). Extensive surface flow visualization studies (using titanium dioxide in the oil with oleic acid) and schlieren photography were carried out to infer flow features on multistep configurations.

E. Measurement Uncertainties

Uncertainties in the measured data estimated using the methodology of Kline and McClintock[18] and considering data repeatability are

$$\Delta C_{DA} = \pm 0.02 C_{DA} \qquad (20\text{–}1)$$

$$\Delta C_{pb} = \pm 0.015 C_{pb} \qquad (20\text{–}1)$$

where C_{DA} is normalized by the forebody cross-sectional area and C_{pb} is the conventional base pressure coefficient with respect to freestream conditions.

IV. Results and Discussion

We present the experimental results of the different components of the total afterbody drag, as influenced by the important geometrical parameters (discussed in Sec. II). The measured drag output from the balance is corrected for the internal force due to the split pressure, and base pressure is assumed uniform in the calculation of the base drag coefficient.

Figures 4–6 show results of base pressure coefficient C_{pb}, afterbody total drag coefficient C_{DA}, and afterbody profile drag coefficient C_{DP} at transonic Mach numbers of 0.7, 0.8, 0.9, and 0.95, and Mach 2.0. The profile drag C_{DP} consists of two components, namely, the base drag due to steps and the contribution due to skin friction ahead of the step. Because the skin friction is a small fraction (typically less than 20% of C_{DP}), C_{DP} essentially represents the drag due to step flows. This is obtained by subtracting the measured base drag from C_{DA} ($C_{DP} = C_{DA} - C_{DB}$). The results shown in Figs. 4–6 bring out the dependence on the two important parameters, namely, l/h and h/δ_0^*.

Observe (Figs. 4–6) that the MSA configuration does offer significant total drag reduction compared to a blunt base: It is as high as 50% at transonic Mach numbers and about 25% at $M_\infty = 2.0$ for the smallest step height ($h = 0.56$ mm) chosen in the present work. The larger the step height h is compared to boundary-layer displacement thickness δ_0^* the lower the drag reduction. This is consistent with our expectation based on available results on single step flows.[13,14]

A. Effect of Step Length

For short steps ($l/h \to 0$), the total afterbody drag C_{DA} can have values as high as the unmodified blunt base, that is, without any step (see Figs. 4–6). Drag levels of $l/h \to 0$ correspond to high base drag condition and arise due to flow separation at the first step itself, as revealed by surface and schlieren visualization (to be discussed in Sec. IV.C). This is not surprising because the shear layer reattachment cannot occur on the step when l is small in relation to h; in such cases, the separated shear layers meet and close in the near wake. The multistep concept is, therefore, ineffective when $l/h \to 0$.

Interestingly, the (maximum) base pressure [measured at the base (Fig. 3)] occurred around $l/h = 4$–6 at the different Mach numbers investigated (Figs. 4–6). As we shall see in Sec. IV.C, the range of l/h also corresponds to the zone of shear layer reattachment for the different steps.

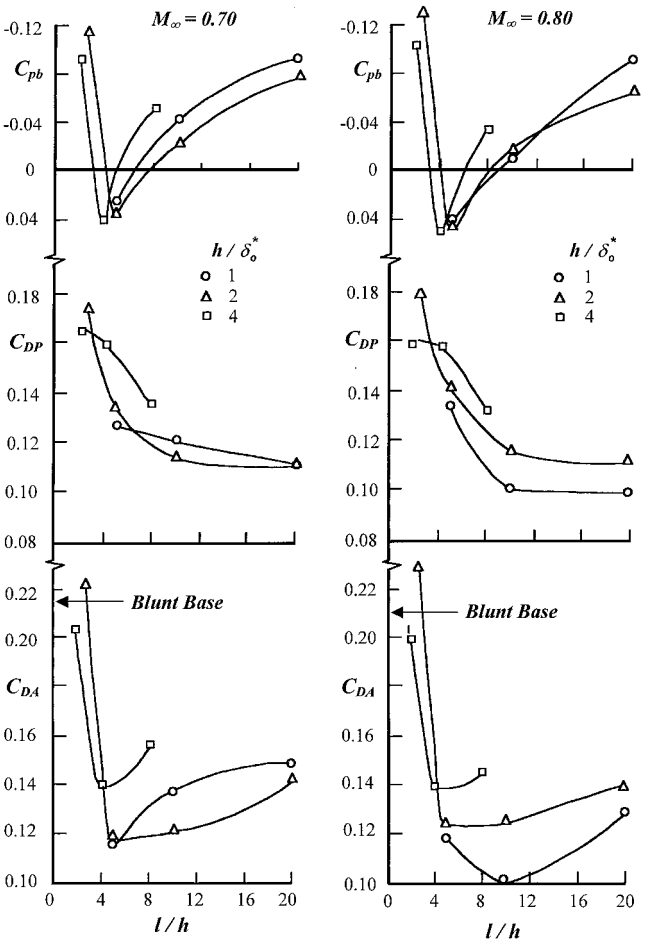

Fig. 4 Base pressure, afterbody profile drag, and total drag characteristics: $M_\infty = 0.70$ and 0.80. (Legend shown is common to all parts of the figure.)

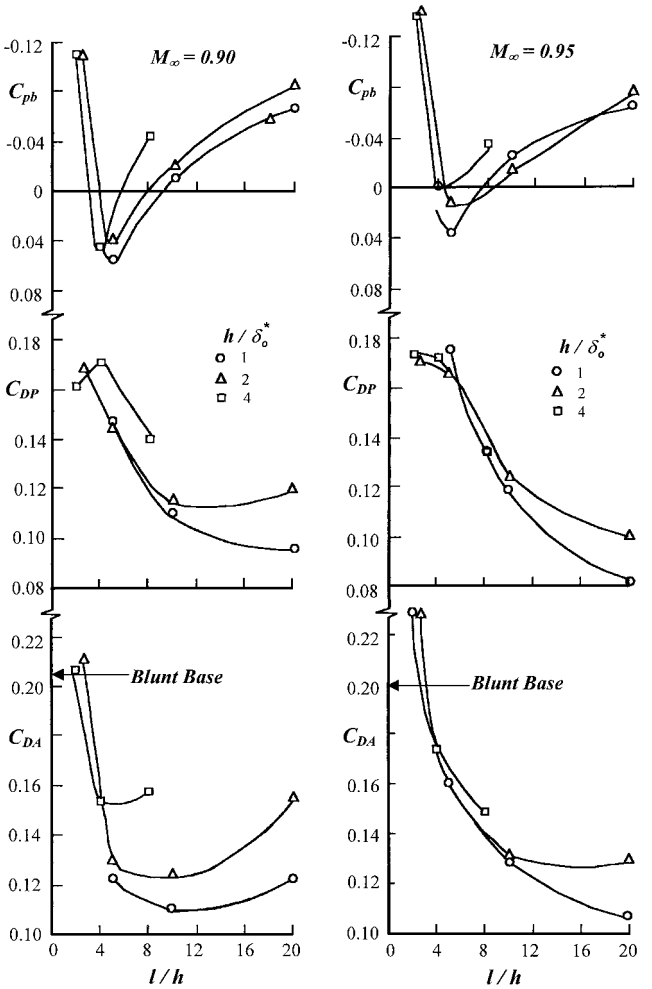

Fig. 5 Base pressure, afterbody profile drag, and total drag characteristics: $M_\infty = 0.90$ and 0.95. (Legend shown is common to all parts of the figure.)

Minimum afterbody total drag, which is relevant from an application or design point of view, is obviously influenced by the variations of C_{pb} (or C_{DB}) and C_{DP} with step length. A useful guideline that emerges from the results shown in Figs. 4–6 is that minimum C_{DA} occurs in the range $l/h = 4$–10 at different Mach numbers except at $M_\infty = 0.95$ (where C_{DA} shows a continuous decrease with l/h).

B. Effect of Initial Boundary-Layer Thickness

The effect of initial boundary-layer thickness has been brought out at the different Mach numbers in Figs. 4–6. It is interesting that both C_{DA} and C_{DP} generally reflect trends that may be expected[13,14] due to the effect of initial boundary-layer parameter h/δ_0^* ahead of the first step; that is, at a given l/h, both C_{DA} and C_{DP} show a gradual decrease with decreasing value of h/δ_0^*. These results suggest that, although the flow past a MSA is complex, involving repeated separation–reattachment processes, the choice of the initial δ_0^* (ahead of the first step) for scaling the step height in design may be appropriate. The larger the boundary-layer displacement thickness δ_0^* is relative to the step height h, the lower the drag that is associated with steps and the total drag of a MSA.

C. Flow Features on MSA

As stated in Sec. II, the flow phenomena on MSA are dominated by boundary-layer separation and reattachment at each step, and the parameter, namely, the ratio of step length to height l/h is a important factor influencing the total drag. Samples of flow features on MSA from surface flow and schlieren visualization are presented in Figs. 7 and 8, respectively. For small values of $l/h(<3)$, the boundary layer separates at the first step (Figs. 7a and 8a) and shear layer closure occurs in the near wake; the step flow is buried in the near-wake separated flow resulting in high drag values [comparable to the blunt base (Figs. 4–6)]. Examples of surface flow

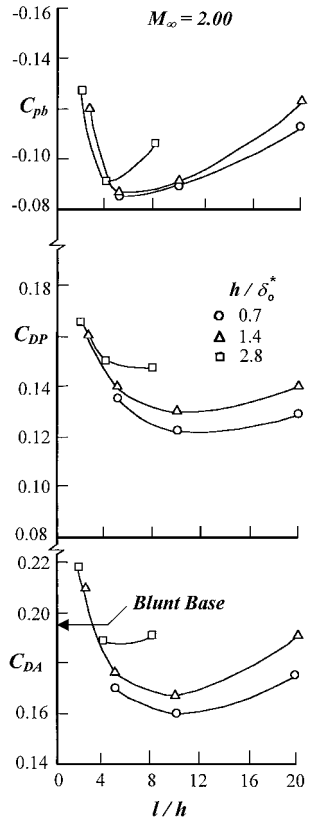

Fig. 6 Base pressure, afterbody profile drag, and total drag characteristics: $M_\infty = 2.0$. (Legend shown is common to all parts of the figure.)

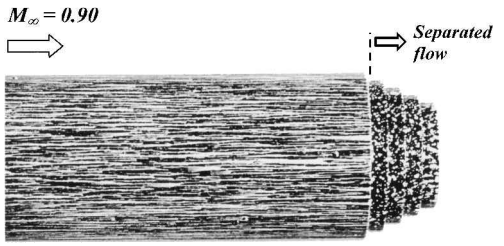

a) Four-step model: $l = 2.5$ mm, $h = 1.125$ mm

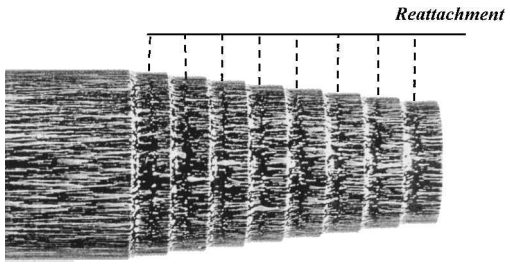

b) Eight-step model: $l = 5$ mm, $h = 0.56$ mm, $x_R/h = 4.1$

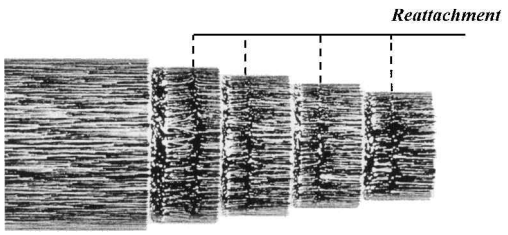

c) Four-step model: $l = 10$ mm, $h = 1.125$ mm, $x_R/h = 4.4$

Fig. 7 Surface flow features on MSA: $M_\infty = 0.90$.

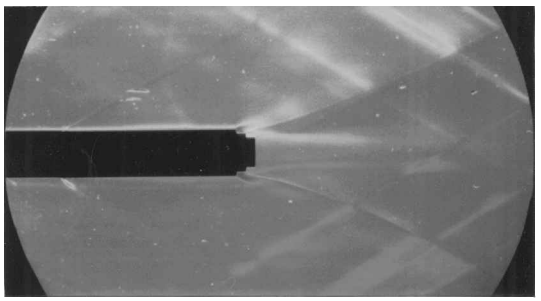

a) Two-step model: $l = 5$ mm, $h = 2.25$ mm, $l/h = 2.22$

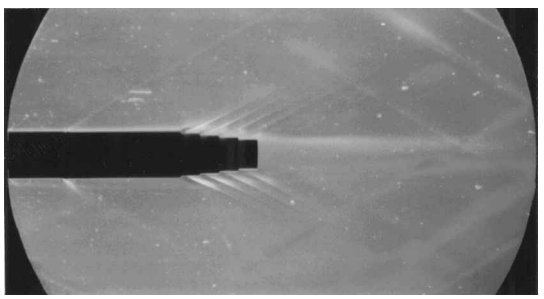

b) Four-step model: $l = 10$ mm, $h = 1.125$ mm, $l/h = 8.88$, $x_R/h = 4.4$

Fig. 8 Schlieren photographs of flow past MSA: $M_\infty = 2.0$.

features presented in Figs. 7b and 7c (and other cases not included here) show that the shear layer reattachment x_R for the different MSA configurations has an average value in the range $4h$–$6h$. Interestingly, the minimum base drag condition ($l/h = 4$–6), therefore, corresponds to the boundary layer on the step surfaces in a nearly incipient reattachment state before subsequent separation at the next step. The range of $l/h = 8$–12, which corresponds to minimum total drag (Figs. 4–6), represents flow conditions with a closed bubble on each step (like flow past a backward facing step) and some recovery of the boundary layer before subsequent separation at the next step. The schlieren photograph at $M_\infty = 2.0$ (Fig. 8b) does reveal features of expansion fan and reattachment shock at each step, as may be expected for a closed bubble. For large $l/h (\geq 12)$, the skin-friction drag following reattachment at each step presumably (due to increased wetted area) contributes to the increased total afterbody drag. It is a difficult task to estimate the skin-friction characteristics in a rehabilitating turbulent boundary layer following reattachment at each step.

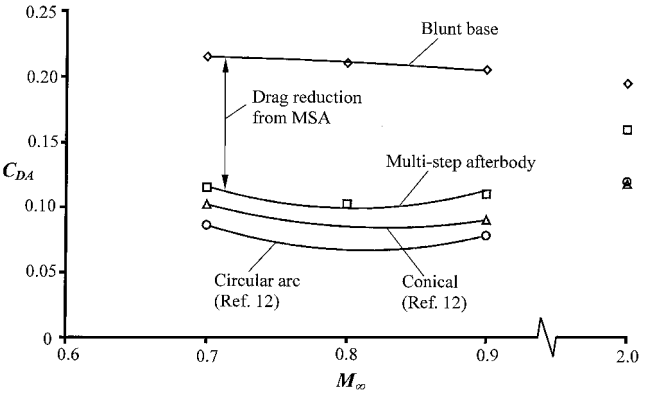

Fig. 9 Drag reduction from MSA and comparision with conical and circular arc boattails.

D. Comparison of Drag Characteristics of MSA with Axisymmetric Boattails

We now compare the measured minimum values of afterbody total drag of MSA against the minimum total drag of axisymmetric boattailed bases having conical and circular arc profiles with the same base area; these results are available in Figs. 5 and 7 of Ref. 12. The drag comparisons are shown here in Fig. 9. Observe that, compared to an unmodified blunt base configuration, MSA offer significant total drag reduction (in the range of 25–50%, depending on freestream Mach number), which is much larger than that reported in the literature.[10,11] However, circular arc boattails have the lowest drag, and the conical boattails fall in between. These results show that, for a given base area, MSA may, in general, have relatively higher total drag compared to axisymmetric boattails. A broad comparison of measured C_{DP} values of MSA (Figs. 4–6) with those on circular arc boattailed models (Fig. 6 in Ref. 12) at $M_\infty = 0.70$, 0.90, and 2.0 indicates that the higher drag of MSA is contributed to appreciably by the drag due to step flows. In essence, the momentum losses associated with separation–reattachment process at each step is a major factor contributing to the increased total drag of multistep configurations.

V. Conclusions

Experiments have been performed at high speeds assessing the drag reduction potential of a class of MSA with a common step height and uniform spacing of steps. The geometrical and flow parameters relevant for the design of MSA have been identified, and a systematic parametric study has been carried out examining the different effects. In particular, the effects of step length, step height, and the initial boundary-layer thickness on drag have been brought out.

The results show that, with a proper design, MSA can offer significant total drag reduction (25–50%) compared to an unmodified blunt base, which is much larger than that reported in the literature. However, compared to conventional axisymmetric afterbodies with circular arc or conical boattails of a given base area, the MSA have relatively higher drag, which is a result of increased momentum losses associated with the separation–reattachment processes at each step. Certain gross flow features on MSA based on flow visualization studies are discussed, and some guidelines useful for the design of MSA for minimum drag have emerged.

The present study has examined only one family or class of MSA, and other designs, for example, involving nonuniform step height

and spacing and possibly a combination of steps and boattailing, could offer larger drag reduction than those reported here.

Acknowledgment

The author sincerely thanks S. R. Patil (Scientist, National Trisonic Aerodynamic Facilities) for his assistance and early association with this work.

References

[1]Tanner, M., "Reduction of Base Drag," *Progress in Aerospace Sciences*, Vol. 16, No. 4, 1975, pp. 369–384.

[2]Viswanath, P. R., "Flow Management Techniques for Base and Afterbody Drag Reduction," *Progress in Aerospace Sciences*, Vol. 32, No. 2/3, 1995, pp. 79–129.

[3]Mair, W. A., "Reduction of Base Drag by Boat-Tailed Afterbodies in Low Speed Flow," *Aeronautical Quarterly*, Vol. 99, 1969, pp. 307–320.

[4]Murthy, S. N. B., and Osborn, J. R., "Base Flow Phenomena With and Without Injection: Experimental Results, Theories and Bibliography," *Aerodynamics of Base Combustion*, edited by S. N. B. Murthy, Vol. 40, Progress in Astronautics and Aeronautics, AIAA, New York, 1976, pp. 7–210.

[5]Murthy, S. N. B., and Osborn, J. R., "Base Combustion Effects on Base Pressure," *Aerodynamics of Base Combustion*, edited by S. N. B. Murthy, Vol. 40, Progress in Astronautics and Aeronautics, AIAA, New York, 1976, pp. 307–338.

[6]Mair, W. A., "The Effect of Rear Mounted Disc on the Drag of a Blunt-Based Body of Revolution," *Aeronautical Quarterly*, Vol. 16, 1965, pp. 307–320.

[7]Viswanath, P. R., "Passive Devices for Axisymmetric Base Drag Reduction at Transonic Speeds," *Journal of Aircraft*, Vol. 25, No. 3, 1988, pp. 258–262.

[8]Kentfield, J. A. C., "Short, Multi-Step Afterbody Fairings," *Journal of Aircraft*, Vol. 21, No. 5, 1984, pp. 351–352.

[9]Ringleb, F. O., "Separation Control by Trapped Vortices," *Boundary Layer and Flow Control*, edited G. V. Lachmann, Pergamon, Oxford, 1961, pp. 265–294.

[10]Wikoff, D., Cottrell, C. J., and Packard, J. D., "An Examination of Controlled Vortex Drag Using Stepped Afterbodies from $M = 0.5$ to 3.0," AIAA Paper 87-0445, Jan. 1987.

[11]Kidd, J. A., "An Investigation of Drag Reduction Using Stepped Afterbodies," AIAA Paper 89-0333, 1989.

[12]Viswanath, P. R., and Patil, S. R., "Zero-Lift Drag Characteristics of Afterbodies with a Square Base," *Journal of Spacecraft and Rockets*, Vol. 34, No. 3, 1997, pp. 290–293.

[13]Hastings, R. C., "Turbulent Flow Past Two-Dimensional Bases in Supersonic Streams," Aeronautical Research Council, Repts. and Memoranda 3401, United Kingdom, Dec. 1963.

[14]Nash, J. F., "A Discussion of Two-Dimensional Turbulent Base Flows," Aeronautical Research Council, Repts. and Memoranda 3468, United Kingdom, July 1965.

[15]Cahn, M. S., "An Experimental Investigation of Sting Support Effects on Drag and Comparison with Jet Effects at Transonic Speeds," NACA Rept. 1353, 1958.

[16]Gloss, B. B., and Sewall, W. G., "Support Sting Interference in Boat-Tail Pressure Drag for Reynolds Number up to 70×10^6," AIAA Paper 83-0387, 1983.

[17]Desai, S. S., and Kiske, S., "A Computer Program to Calculate Turbulent Boundary Layer and Wake in Compressible Flow with Arbitrary Pressure Gradient Based on Green's Lag Entrainment Method," Inst. for Thermo and Fluid Dynamics, Rept. 89/1982, Ruhr Univ., Bochum, Germany, Jan. 1982.

[18]Kline, S. J., and McClintock, F. A., "Describing Uncertainties in Single Sample Experiments," *Mechanical Engineering*, Vol. 75, No. 1, 1953, pp. 3–8.

P. R. Bandyopadhyay
Associate Editor